Ascorbic Acid-Sensitized Au Nanorods-functionalized nanostructured TiO_2 Transparent Electrodes for Photoelectrochemical Genosensing

Francesca Bettazzi[1], Serena Laschi[1], Diego Voccia[1], Cristina Gellini[1], Giangaetano Pietraperzia[1], Luigi Falciola[2*], Valentina Pifferi[2], Anna Testolin[2], Chiara Ingrosso[3*], Tiziana Placido[3], Roberto Comparelli[3], M. Lucia Curri[3], Ilaria Palchetti[1*]

[1]Dipartimento di Chimica, Università degli Studi di Firenze, Via della Lastruccia 3, 50019, Sesto Fiorentino, (Fi), Italy; [2]Dipartimento di Chimica, Università degli Studi di Milano, via Golgi 19, 20133, Milano, Italy; [3]CNR-IPCF Istituto per i Processi Chimici e Fisici, Sez. Bari, c/o Dip. Chimica Via Orabona 4, 70126 Bari, Italy; * INSTM, Via G. Giusti 9, 50121 Firenze (Italy)

Abstract

Au nanorods (NRs) modified nanostructured TiO_2/ITO electrodes have been fabricated and characterized in order to develop a biosensing platform for the photoelectrochemical determination of microRNAs. The proposed method is based on the use of thiolated DNA capture-probes (CPs) immobilized onto Au NR surface. The Au NRs are chemically bound at the surface of TiO_2/ITO electrodes by means of the mercaptosuccinic acid linker. Subsequently, the DNA CPs are bound to the Au NR surface through the thiolate group, and reacted with the target RNA sequence. Finally, the obtained biosensing platform is incubated with alkaline phosphatase and L-ascorbic acid 2-phosphate (AAP) enzymatic substrate, for the *in situ* generation of ascorbic acid (AA). Such AA molecule, coordinating to surface Ti atoms, generates a charge transfer complex, that results in a shift of the UV absorption threshold toward the visible spectral region of the nanostructured TiO_2 forming the electrode and, hence, in the occurrence of an absorption band centered at 450 nm. The photoelectrochemical monitoring of the formation of the AA-TiO_2 complex, under the visible light of a commercial LED light source, allows the selective and quantitative detection of the target microRNA strands.

Keywords: photoelectrochemical, nanostructured TiO_2, Au nanorods, nucleic acid, ascorbic acid, small RNAs

1. Introduction

Recently, photoelectrochemical (PEC) biosensors have emerged as particularly attractive options among the different biosensing methods. Photoelectrochemical approaches possess advantages of both optical and electrochemical methods by coupling light excitation and electrochemical detection, and thus resulting potentially very sensitive [1] due to the low background current. Moreover, while the all-optical detection methods, such as fluorescence, require complex and expensive optical imaging devices and sophisticated image recognition software, the inherent low cost of the electrochemical instrumentation makes the PEC method simple, rapid and cost effective [2]. Recently, due to the emergence of novel photoelectrochemically active species and new detection schemes, photoelectrochemistry has received increasing attention in biosensing of proteins [3], as well as in the development of hybridization assay [4–9] for the recognition of specific nucleic acid sequences.

In this work, the PEC properties of nanostructured TiO_2 modified ITO electrodes, decorated with colloidal Au nanorods (NRs) have been investigated for the development of a PEC biosensing platform for the determination of small RNAs, known as microRNAs, under visible light illumination. CTAB-capped Au NRs have been synthesized by means of a colloidal chemical route, which is able to control NR size and geometry. The surface of the optically transparent nanostructured TiO_2 electrodes has been modified by immobilizing mercaptosuccinic acid (MSA), which acts as a linker for anchoring the Au NRs. Au nanoparticles, either isotropic or anisotropic, as the NRs, are particularly suited for conjugation with biomolecules [10], preserving their biological activity. Moreover, increasing the surface-to-volume ratio, they represent a powerful tool to modify electrode materials and to construct robust and sensitive biosensors [11]. Thus, the thiolated nucleic acid capture probes (CPs) have been immobilized on the Au NRs and allowed to hybridize with the target biotinylated microRNA sequences. The enzyme alkaline phosphatase (AP) has been used as a label for the biorecognition, since it generates ascorbic acid (AA), that binding to the TiO_2 surface enable its photosensitization and ultimately the detection and quantization of the microRNA (Scheme 1). MicroRNAs (miRNAs) are endogenous, evolutionarily conserved, non-coding RNA molecules of about 20 nucleotides in length, functioning as posttranscriptional gene regulators. They regulate a wide range of biological functions, from cell proliferation and death to cancer progression. The importance of miRNA function suggests that their expression may provide a valuable diagnostic indicator as a cancer biomarker. However, the short nature of miRNA sequences greatly complicates the use of standard molecular biology method based upon PCR. Therefore, significant efforts have been

devoted to the development of innovative analytical methods and, recently, photoelectrochemical genosensing platforms have been extensively studied [4–9]. Different electrode materials, including Bi_2S_3 NRs [4,5,8], graphite-like C_3N_4 [6], or CdS modified carbon nanotubes [9] have been used, in presence of AA as electrondonor. TiO_2 nanostructures hardly have found a direct application in PEC biosensing, since TiO_2 only absorbs UV-light, that is a type of radiation that can damage biomolecules and requires expensive, highly maintenance and demanding sources typically used for generating exciton in its wide band gap (ca. 3.2 eV) [12]. In order to overcome such a limitation, coupling of TiO_2 with narrow-band gap semiconductors or with organic photosensitizer has been performed, [13–16] in order to shift its absorption in the visible spectral range. In this work, the possibility of exploit *in situ* enzymatically generated AA for genosensing has been studied. AA is a well-known electron donor that has been widely studied in solar energy conversion systems [12,17,18]. Indeed, the surface modification of the nanostructured TiO_2 electrodes with AA, leads to the TiO_2 photosensitization, through the formation of a charge-transfer complex, that ultimately shifts the photoresponse of TiO_2 up to 500 nm [12,17]. In particular, a bidentate chelate binding of AA, through the two ene-diolate oxygen atoms, with the anionic oxygen as electron donor, is assumed responsible of the formation of the charge-transfer complex in the form of a chelate ring structure. Remarkably, such a photosensitization process of the Au NR surface modified nanostructured TiO_2 electrodes, occurs only upon AA generation from the enzymatic reaction labeling the hybridization event, thus allowing the PEC detection of the miRNA target sequence, under visible-light illumination. The photocurrent spectrum of the TiO_2 film, sensitized by AA, is characterized by a maximum located at $\approx$ 450 nm. Such a photocurrent is due to a rapid visible light-induced electron injection from AA into the conduction band of TiO_2. The preliminary results of the developed genosensor for miRNA determination indicate the reliability of the proposed approach. The obtained results demonstrate that the miRNA detection can be accomplished by using a compact analytical device, equipped with a LED-light source, that allows the accomplishment of a prototype compliant with the requirements and the characteristics of a point of care testing (POCT).

2. Experimental

2.1. Reagents

Dithiothreitol (DTT), 6-mercapto-1-hexanol (MCH), streptavidin–alkaline phosphatase (S2890, Strept-AP, 2:1 conjugation stoichiometry), diethyl pyrocarbonate (DEPC), ascorbic acid (AA), L-ascorbic acid 2-phosphate trisodium salt (AAP), mercaptosuccinic acid (MSA), bovine serum albumin (BSA), Tris–HCl, sodium borohydride ($NaBH_4$, ~99%), hydrogen tetrachloroaurate(III) trihydrate ($HAuCl_4 \cdot 3H_2O$, 99.9%), silver nitrate ($AgNO_3$, 99.9999%), were obtained from Sigma–Aldrich (Milan, Italy). Disodium hydrogen phosphate, sodium dihydrogen phosphate, magnesium and potassium chloride were purchased from Merck (Milan, Italy). NAP-10 columns of Sephadex G-25 were obtained from Amersham Pharmacia Biotech (Uppsala, Sweden). Nanostructured TiO_2/ITO electrodes were purchased from Solaronix (Aubonne, Switzerland). MilliQ water (DEPC treated for RNA analysis) was used throughout this work.

Synthetic oligonucleotides were obtained from MWG Biotech AG (Germany), namely:

probe (DNA-SH): 5' GAA-ACC-CAG-CAG-ACA-ATG-TAG-CT – SH 3',

target (miRNA 221): 5' AGC-UAC-AUU-GUC-UGC-UGG-GUU-UC –biotin 3',

non-complementary (miRNA 16): 5′ UAG-CAG-CAC-GUA-AAU-A-biotin-3′

Prior to use, the thiol-modified oligonucleotides were treated with DTT. This reagent allowed reduction and cleavage of oligo dimers eventually obtained by oxidative coupling of two DNA-SH molecules (i.e. DNA-S-S-DNA). The lyophilized oligonucleotides were dissolved in a 10 mM Tris-HCl buffer solution (pH 8.3) containing 20 mM of DTT. The reaction was allowed to proceed for 2 h at room temperature. The thiolated DNA was then purified by elution through a NAP-10 column of Sephadex G-25 using 0.5 M phosphate buffer (pH 7.4). DNA-SH stock were prepared in the same buffer and stored frozen.

Human serum type AB (Sigma– Aldrich (Milan, Italy) was diluted 1:100 (v/v) in Tris buffer and filtered (0.45 μm).

2.2. Synthesis and characterization of CTAB–coated Au NRs

CTAB–coated Au NRs were prepared by using the seed-mediated growth method [19] reported in literature. The synthesis relays on two steps: firstly, a seeds solution containing CTAB-stabilized Au NPs (< 3 nm) was prepared by reducing an Au precursor, $HAuCl_4 \times 3H_2O$ (5 mL, 5×10^{-4} M), with $NaBH_4$ (0.01 M) in CTAB (5 mL, 0.2 M), and then kept under vigorous stirring for 2 h. Next, a growth solution of Au NRs was prepared: 8.5 mg of $AgNO_3$, 18.22 g of CTAB and 100 mg of $HAuCl_4 \times 3H_2O$ were dissolved in 500 mL of deionized water. This mixture was kept at room temperature under continuous stirring. Then, 7 mL of a 0.0778 M aqueous solution of AA were added dropwise to the above mixture.

When the mixture becomes colorless (indicative of the reduction of Au(III) to Au(I)) [19], 0.8 mL of the seed solution was added to the growth solution and a dark-red color developed within 10 min [20]. After preparation, cycles of centrifugation were performed at 7000 rpm for 20 min, to wash the Au NRs to discard uncoordinated CTAB.

CTAB-coated Au NRs were optically and morphologically characterized by means of UV-Vis absorption spectroscopy and Trasmission Electron Microscopy (TEM). UV−Vis absorption spectra of solutions of the as prepared Au NRs were recorded at room temperature, by using a Varian Cary 5000 UV−Vis−NIR scanning spectrophotometer in the 300−1200 nm range.

TEM analyses were performed with a Jeol JEM-1011 microscope, operating at 100 kV. The specimens were prepared by depositing few drops of aqueous Au NR dispersions onto a carbon-coated copper grid and then allowing the solvent to evaporate.

2.3. Modification and characterization of the nanostructured TiO_2/ITO electrodes by Au NRs

Commercial nanostructured TiO_2/ITO electrodes were surface modified with CTAB-capped Au NRs, by using mercaptosuccinic acid (MSA) as a linker molecule. Namely, the TiO_2/ITO electrodes were incubated for 24 h in a 1 M solution of MSA, and then, in a 6×10^{-9} M solution of CTAB-coated Au NRs at pH 9, for 3 h.

The bare TiO_2/ITO electrodes and the prepared AuNRs/MSA/TiO_2/ITO electrodes were morphologically characterized by Field Emission Scanning Electron Microscopy (FE-SEM) by using a Zeiss Sigma microscope, equipped with an in-lens secondary electron detector and an INCA Energy Dispersive Spectroscopy (EDS) detector. Samples were mounted onto stainless-steel sample holders by a double side carbon tape and grounded by silver paste.

2.4. Thiolated DNA Capture-probe (CP) immobilization

AuNRs/MSA/TiO_2/ITO electrodes were exposed to 20 μL of the thiolated oligonucleotide solution (10 μM in 0.5 M phosphate buffer, pH =7.2). Chemisorption was allowed to proceed overnight (≈ 16 h). During incubation, the electrode cell was covered with parafilm in order to prevent the evaporation of the oligonucleotide solution. The immobilization step was followed by incubation with 20 μL of 1 mM 6-mercapto 1-hexanol (MCH) aqueous solution for 1 h. Such a step intends to modify Au NP surface active sites and avoid non specific adsorption of biotinylated target strands, increasing hybridization efficiency [21]. Prior to

hybridization reaction, the modified electrode was washed twice with 0.5 M phosphate buffer pH 7.2 (PB).

2.5. Hybridization and labeling

The probe-modified electrode was then exposed to a 20 μL of the biotinylated target sequence in PB solution for 20 min. After hybridization, the sensor was washed twice with 10 mM Tris-HCl buffer, pH 9.8. The biotinylated hybrid obtained at the electrode surface was reacted with a 20 μL solution containing 4 U/mL of the streptavidin-alkaline phosphatase conjugate and 10 mg/mL of BSA, as blocking agent [21], in 10 mM Tris buffer, pH= 9.8.
After 20 min, the sensor was washed twice with Tris buffer. The photoelectrochemical cell was then filled with 100 μL of an L-ascorbic acid 2-phosphate (AAP) enzymatic substrate solution (10 mg/mL in 10 mM Tris buffer, pH =9.8). After 20 min of incubation, photocurrents were amperometrically detected.

2.6. Electrochemical and Photoelectrochemical Characterization and Detection

Electrochemical measurements were performed with an Autolab PGSTAT10 computerized electrochemical system equipped with the FRA2 frequency response analyzer and controlled by GPES 4.9 software (EcoChemie). A Pt wire, Ag/AgCl wire, and AuNRs/MSA/TiO_2/ITO disk served as the auxiliary, pseudo-reference, and working electrode, respectively. The electrodes were mounted in a customized cell constituted of two parts forming a Plexiglas box, as reported in Scheme 2. The modified sensor was located in a slot created on the bottom part of the cell while two screws allowed fixing the top part, where a cylindrical well housed both illumination system and solution. The electrode geometric area was 0.2 cm^2. The distance of the LED from the electrode surface defines a cell volume of 100 μL. An O-ring controlled the tightness at the electrode surface. For the PEC characterization of the bare TiO_2/ITO, of the MSA/TiO_2/ITO and AuNRs/MSA/TiO_2/ITO electrodes, an ozone free Xenon lamp emitting in the 200-2000 nm range (450 W, Orion) coupled with a monochromator (Jobin-Yvon) was used as a light source with an average emission power of 100 μW/cm^2. A series of mirror and glasses were used in order to direct the light on the working electrode surface.
For miRNA determination, AA photocurrents, at 0 V vs Ag/AgCl, were amperometrically detected as the analytical signal, under illumination with a commercial white LED (3 mm white LED, Nichia Corporation) emitting in the visible range 400-700 nm with maxima at 456 and 549 nm (Figure S1), respectively, and intensity in the mW/cm^2 order. All

photoelectrochemical measurements were referred to the Ag/AgCl wire reference electrode at room temperature (25°C). It should be noted that a new CP-modified PEC biosensor was used for each tested miRNA concentration.

Cyclic Voltammetry (CV) measurements were performed at different scan rate in 0.1 M KCl solution. Electrochemical Impedance Spectroscopy (EIS) measurements were performed with E_{dc} in the range from - 0.2 to + 0.8 V, every 0.1 V with the parameters showed in Table S1. Each spectra was fitted by using ZView software.

The flat band potential, E_{fb}, and donor density, N_D, were obtained from Mott – Schottky equation [22]

$$\frac{1}{C^2} = \frac{2}{e\varepsilon\varepsilon_0 A^2 N_D}\left(E - E_{fb} - \frac{k_B T}{e}\right) \qquad \text{[Eq.1]}$$

where C and A are the interfacial capacitance and electrode surface area, respectively, E the applied voltage, k_B is Boltzmann's constant, T the absolute temperature, ε is the dielectric constant of the semiconductor, ε_0 is the permittivity of a free space (vacuum) and e is the electronic charge. Therefore, a plot of $1/C^2$ against E should yield a straight line from which E_{fb} can be determined from the intercept on the E axis. The value of N_D can also be conveniently evaluated from the slope knowing ε and A of the electrode.

The values for $1/C^2$ were obtained from EIS data by using the following equation:

$$\frac{1}{C^2} = \left(\frac{-Z''^2 + (Z' - R_\Omega)^2\omega}{-Z''}\right)^2 \qquad \text{[Eq.2]}$$

where R_Ω is the cell resistance, Z' and Z'' the impedance values registered at the chosen angular frequencies ω ($2\pi f$, with f = 1000, 100, 10 Hz).

3. Results and discussion

3.1. Electrochemical and photoelectrochemical characterization of the nanostructured TiO_2/ITO electrodes

The TiO_2/ITO electrode was electrochemically characterized in view of its application as a platform for AA PEC detection. Electrochemical impedance spectroscopy, a valuable technique to characterize the electrochemical behavior of semiconductor electrodes in an electrolyte solution, was employed at different applied voltage bias, ranging from – 0.2 V to + 0.8 V *vs.* Ag/AgCl. For all the potentials the complex plane plots (Figure 1a) show two semicircles, fitted with the equivalent circuits represented in Figure S2. In particular, the cell

resistance R_Ω is in series with two consecutive resistances and constant phase elements in parallels. The constant phase elements (CPE) describe the charge separation and are modelled as $[(Ci\omega)^{\alpha}]^{-1}$, representing a pure capacitance for $\alpha=1$ and a non-ideal capacitance for $0.5<\alpha<1$. R_1 and CPE_1 refer to the resistance and capacitance related to the TiO_2-electrolyte solution interphase, while R_2 and CPE_2 to the TiO_2-ITO interphase. The values obtained from the fitting are reported in Table S2. The cell resistance (R_Ω) is in general not influenced by the voltage variation, while the other parameters change, especially at negative potentials. This phenomenon is due to the proximity with the TiO_2 flat band potential (evaluated in the next paragraph) for R_1 and CPE_1 and with the tin reaction of ITO [23] for R_2 and CPE_2. Moreover, R_1 are really lower than R_2, since they are related to a solid-liquid and to a solid-solid interphase, respectively. Finally, α_1 is lower than 1, showing a non-ideal capacitive behavior for the electrolyte-TiO_2 interphase, probably ascribable to the nanoporous surface morphology of the electrode (Figure S3). The situation is different in the case of ITO-TiO_2 interphase, with α_2 very close to 1, due to a more homogeneous structure of ITO. The study of capacitance variation at different chosen frequencies allows to describe the relationship between semiconductor and electrolyte energy levels, correlating it to the *flat band potential* (E_{fb}) of the semiconductor through the Mott – Schottky equation (Eq. 1) [23].

Figure 1b displays the Mott–Schottky diagram of $1/C^2$, as a function of the applied voltage bias at different frequencies (see the experimental part for further details), from which a positive slope was observed, confirming a *n-type* semiconductor behavior. Furthermore, the plot was extrapolated to ($1/C^2 = 0$) to estimate, by following Eq. [1], the value of E_{fb}, namely (– 283 ± 40 mV), that is in agreement with the data reported in literature [24], [25]. In addition, the carrier density (or doping level N_D) was calculated, assuming ε for TiO_2 equal to 173 [26], $\varepsilon_0 = 8.85\ 10^{-12}$ F/m [27], A = 0.2 cm^2 (0.5 cm diameter) and $e = 1.6 \cdot 10^{-19}$ C, giving $N_D = 2.7 \cdot 10^{22}$ cm^{-3}, in accordance to the literature value for N_D that is in the range of 10^{18} to 10^{23} cm^{-3}, depending on the TiO_2 nanostructured film thickness and the electrolyte used [28].

The above results have been obtained considering the Mott-Schottky data linear part closer to the potential axis. Above +0.1 V a non-linear trend is evinced, already observed in the literature [29],[30], which could be due to different factors: non-uniform distribution of donors; dielectric relaxation phenomena due to surface structure inhomogeneity and film amorphous nature [29]. However, the real nature of these behaviors is still to be clarified.

CV of the TiO_2/ITO electrodes were also recorded in the presence of 0.1 M KCl, at three different voltage scan rates, as shown in Figure 1c. All voltammograms show a large

potential range where the current is only capacitive (between - 0.2 to + 0.8 V). In this range, the absence of faradaic phenomena on the electrode surface preserves the electrode from any modification. Figure 1d shows CV measurements performed in 0.1 M KCl in presence and absence of 10 mM AA. From the voltammograms, the potential range, where faradaic phenomena are absent, is approximately between - 0.1 and + 0.2 V vs Ag/AgCl.

3.2. Nanostructured TiO_2/ITO photoanode modification with the Au NRs

CTAB-coated Au NRs were synthetized by following the procedure reported in [19], [31] and characterized by UV-Vis absorption spectroscopy and TEM investigation. Figure 2a reports a typical UV-Vis absorbance spectrum of anisotropic Au nanoparticles. In particular, it is possible to distinguish two absorption bands, the former due to light absorption along the short axis at ca. 500 nm and the latter due to absorption along the long axis at ca. 800 nm. Inset of Figure 2a shows a TEM micrograph attesting for the formation of Au NRs having average sizes of 55 ± 7 and 17 ± 2 nm.

Immobilization of the CTAB-coated Au NRs on the nanostructured TiO_2/ITO electrode was performed by using MSA as an anchoring molecule. The –COOH moiety of MSA is expected to coordinate in a bidentate chelating bond the TiO_2 electrode surface, whereas –SH groups bind the Au NR surface. Figure 2b reports the SEM micrograph of a TiO_2/ITO supporting electrode surface modified by Au NRs, while the SEM image of the bare nanostructured TiO_2/ITO electrodes are reported in Figure S3. The secondary electron microscopy investigation shows that, after the incubation of the MSA/TiO_2/ITO electrode in the solution of the CTAB-capped Au NRs, the nanoporous surface of the TiO_2 electrode is coated with highly bright elongated nanostructures, characterized by a morphology compatible with that observed for the CTAB-coated Au NRs in the TEM micrograph (Figure 2a, inset).

CVs recorded at AuNRs/MSA/TiO_2/ITO electrode in 0.1 M KCl, in absence (i) and presence (ii) of 10 mM AA, are reported in Figure 2c. The electrochemical oxidation of AA starts at potential value higher than + 0.2V. Instead, in the potential window between - 0.1 - + 0.1 V, faradaic phenomena are absent, confirming that the current is capacitive. The inset of Figure 2c shows an enlargement of the CV recorded at the at AuNRs/MSA/TiO_2/ITO electrode (iii) in comparison to the CV recorded at the MSA/TiO_2/ITO electrode (iv), confirming that the current is capacitive, in this potential window, for both electrodes. Thus, 0 V was the potential chosen for recording photocurrents in presence of AA.

Figure 2d reports the photocurrents of the pristine TiO_2/ITO, of the MSA/TiO_2/ITO and of AuNRs/MSA/TiO_2/ITO electrodes, respectively, as a function of the selected illumination

wavelength range between 300-600 nm. The experiments were performed in Tris buffer, under the applied potential of 0 V vs Ag/AgCl. The figure shows for the bare TiO_2/ITO electrodes a maximum of photocurrent at 350 nm of 5.6 ± 0.4 μA, which decreases of ≈ 13 % down to 4.9 ± 0.3 μA, in the MSA/TiO_2/ITO photoanode, attesting for a slightly lower photoactivity of the electrode after immobilization of the MSA linker. By contrast, the AuNRs/MSA/TiO_2/ITO electrodes exhibit a significant decrease of the photoactivity in the UV range, namely of ≈ 49% at 350 nm, with a photocurrent of 2.8 ± 0.1 μA, that is substantially lower than that of pristine TiO_2/ITO. Such a decrease could be reasonably due to a resistive behavior of the CTAB organic layer coating the Au NRs, responsible for a shielding effect towards the TiO_2/ITO surface. The photocurrents of all electrodes are negligible in the visible light spectral range in the absence of AA (Figure 2d), and are not affected by the direction of the wavelength scan (data not shown).

Finally, Figure 3 reports the photocurrents of the AuNRs/MSA/TiO_2/ITO electrodes, recorded at 0 V vs Ag/AgCl, at increasing concentration of AA, at different wavelengths in the 300-600 nm range. Figure 3a shows a decrease of the photocurrent value at 350 nm with the increase of the AA concentration, and concomitantly, an increase of the photocurrent in the range of wavelengths between 400 - 600 nm, with a local maximum centered at ≈ 450 nm. The increase of the photocurrent in the visible spectral region can be attributed to the occurrence of a charge transfer complex, due to the binding of AA at the surface of TiO_2/ITO electrode. It has been reported that the chelation of Ti^{4+} with ascorbic acid, which is a well-established phenomenon that takes place via two hydroxyl groups by proton elimination, results in a sensitization process, due to the shift of the absorption threshold of the TiO_2 electrodes up to ≈1.2 eV toward the visible region [18]. Moreover, in concomitance to the increase of the photocurrent at 450 nm, a decrease of the photocurrent value at 350 nm, increasing the AA concentration, was observed, thus further proving the electrode surface modification and the charge-transfer complex formation, extending the absorption towards the visible spectral range. Remarkably, the extent of the complex formation and hence the intensity of the related photocurrent, depend on the concentration of AA.

Upon exposure to AA, the surface of the sensor was regenerated with a simple washing step with demineralized water. Figure 3a (-◄-, 0 mM AA, clean) clearly points out that the photocurrent signal recorded after rinsing of the AuNRs/MSA/TiO_2/ITO electrode with demineralized water is almost the same as that recorded before exposure to AA, thus demonstrating the full recoverability of the PEC performance of the electrode. Indeed, after

photoelectron injection, AA is oxidized to dehydroascorbic acid (DHAA), that subsequently is desorbed from the electrode surface by rinsing [12].

The inter-electrode reproducibility was assessed by measuring the photocurrents at AuNRs/MSA/TiO_2/ITO electrodes, under UV illumination at 0 V. A RSD% of 22% (n=3) was obtained.

Further experiments were performed in order to evaluate the AA concentration-dependent behavior of the photocurrent, under illumination of a commercial white LED light. To perform the measurements, the photoanode was mounted on *ad hoc* developed electrochemical cell housing both illumination system and solution (Scheme 2). The results show the linear dependence of the photocurrent (Figure 3b), recorded under the white LED light source illumination, as a function of the AA concentration, investigated in the range of 0.1 mM - 10 mM in Tris Buffer.

3.3. PEC Hybridization assay

Integration of the AuNRs/MSA/TiO_2/ITO photoanode into a PEC biosensor for small RNA detection was achieved via a surface functionalization process of Au NRs by a thiolated CP. The scheme of the assay is shown in Scheme 1. The capture-probe-modified electrode was reacted with the analyte, the biotinylated target miRNA. Then, the biotinylated hybrid was exposed to the alkaline-phosphatase-streptavidin conjugate and phosphorylated ascorbic acid (AAP). AAP acts as a substrate of the biocatalytic reaction leading to the generation of AA. Such a product of the enzymatic reaction was photoelectrochemically monitored by using amperometry under white LED light illumination. The immobilization of the CP has been monitored by the photocurrent measurements. Indeed, the binding of CP on the AuNRs/MSA/TiO_2/ITO electrode is confirmed by the decrease of the photocurrent response, generated in presence of AA (Figure 4a). Such a decrease in the photoelectrochemical current intensity is ascribed to both enhanced steric hindrance and electrostatic repulsion of the negatively charged DNA strands against the diffusion of AA to TiO_2, thus impeding the charge complex formation. The photocurrent has been monitored also after binding of the target and of the alkaline-phosphatase-streptavidin conjugate to CP (CP/10 nM target miRNA/ALP) (Figure 4b). In the absence of enzymatic substrate, the electrode exhibited a response (curve ii) lower than that of the bare electrode (curve i), in agreement with the literature reports [32], [33], and due to the bio-layer architecture that increased the steric hindrance effect and decreased the electron transfer efficiency. The addition of the enzyme substrate, AAP, causes AA generation and, accordingly, an increase in the photocurrent

intensity at 450 nm (iii), confirming the presence of confined ALP, and thus the feasibility of the functionalization protocol. In order to exclude any spontaneous hydrolysis of AAP, the biosensor was washed with 0.5 M PB, and exposed for 30 min to a 0.5 M PB solution in absence and in presence of 10 mg/mL AAP. Phosphate ions present in solution naturally inhibit the enzyme alkaline phosphatase, avoiding AA production. Photocurrents generated in the experiments (curve iv) are comparable to those obtained in absence of AAP (the enzymatic substrate), thus ruling out the occurrence of the spontaneous hydrolysis.

This photocurrent variation can be, thus, exploited for detecting the hybridization reaction. The analytical performances of the photoelectrochemical assay were evaluated by designing a calibration experiment (Figure 4c-d). The obtained CP-modified PEC biosensor was tested for different miRNA concentrations, under the conditions reported in the materials and methods section, demonstrating a linear response, with an estimated limit of detection (LOD) of approximately 20 fmole in 10 μL of sample solution, calculated using a criterion of the background signal plus three times its standard deviation, and a sensitivity of 1.85 nA/nM. The relative standard deviation (RSD) for five consecutive measurements of 10 nM target miRNA was 5% (n=5) with ≈20 nA average anodic current. A typical calibration curve is shown in Figure 4d with relative amperograms in Figure 4c.

The selectivity of the photoelectrochemical genosensor has been investigated by using a miRNA sequence (miRNA 16) that markedly differs from miRNA 221 (the target sequence). Therefore, it can be regarded as a fully non-complementary sequence. Figure 4d shows clearly that the photocurrent response, due to the nonspecific sequence, is lower than that achieved with the specific binding of the target sequence. Reciprocal selectivity of miRNA221 and miRNA222, which is a sequence structurally closely related to miRNA 221 and frequently overexpressed in the same human malignancies, was reported in a previous study [34].

Preliminary results on real matrices, performed by analyzing AA spiked samples, demonstrated the possibility to perform the photocurrent measurements in diluted serum samples. Thus, further research will be aimed to optimize the experimental conditions in order to improve the analytical performance and carry out analysis on real samples. Recently, a procedure to label microRNAs with biotin for the development of an electrochemical genosensor was reported [34]. This procedure should be further implemented and coupled to the proposed photoelectrochemical assay to analyze miRNAs in serum samples. Finally, the possibility to use nanoarchitectures rich in enzyme labels [35], [36] will be evaluated in order to increase the sensitivity.

4. Conclusions

Nanostructured TiO_2/ITO electrodes were modified and characterized for miRNA detection in a photoelectrochemical enzymatic amplification route. After preliminary electrochemical and photoelectrochemical characterizations of bare TiO_2/ITO electrodes, showing their *n-type* semiconductor properties, Au NRs were immobilized on the TiO_2/ITO electrode surface by using MSA as a linker molecule. The modified electrode based on AuNRs/MSA/TiO_2/ITO was further functionalized with CP for subsequent target hybridization. For this purpose, the ALP catalytic activity was exploited for the *in situ* AA generation, starting from AAP. The AA coordination to the TiO_2 surface enabled the semiconductor sensitization, thus ultimately allowing the quantitative determination of the target sequence in the visible spectral range. Such a novel procedure has been demonstrated effective in a genosensing mechanism for the specific determination of a model target miRNA sequence, miRNA 221, a sequence present in many types of lung and breast cancer. Photocurrents at different wavelengths were evaluated in order to demonstrate the generation of a photocurrent in the visible region, avoiding expensive, dangerous and high maintenance UV light sources. A calibration plot in the 0-50 nM range of miRNA was performed, by using a commercial white LED with a power emission in the mW/cm^2 range. The enzyme amplification produces a sensitivity of 1.85 nA/nM, with an estimated LOD of 20 fmole and an average RSD of 5%. LOD estimated should be considered high for many specific applications, but the possibilities to develop new assay scheme with nanoarchitectures rich in enzyme molecules could further increase the sensitivity of the method. This method is not limited to only hybridization assay, but it can also be extended to other applications and other affinity assay. The investigated assay, demonstrates the possibility to develop a simple detection scheme with commercial semiconductor electrodes and commercial low cost light sources.

Acknowledgements

This work was supported by Ministero dell'Istruzione, dell'Università e della Ricerca (MIUR) in the framework of PRIN 2012 (Grant No.20128ZZS2H) and by Ente Cassa di Risparmio di Firenze project ID PED 8780 2014.0757A2202.0734.

References

[1] W.-W. Zhao, J.-J. Xu, H.-Y. Chen, Photoelectrochemical bioanalysis: the state of the art, Chem. Soc. Rev. 44 (2015) 729–741. doi:10.1039/C4CS00228H.

[2] D. Voccia, I. Palchetti, Photoelectrochemical Biosensors for Nucleic Acid Detection, J. Nanosci. Nanotechnol. 15 (n.d.) 3320–3332. doi:doi:10.1166/jnn.2015.10039.

[3] X. Li, L. Zhu, Y. Zhou, H. Yin, S. Ai, Enhanced Photoelectrochemical Method for Sensitive Detection of Protein Kinase A Activity Using TiO2/g-C3N4, PAMAM Dendrimer, and Alkaline Phosphatase, Anal. Chem. 89 (2017) 2369–2376. doi:10.1021/acs.analchem.6b04184.

[4] H. Yin, M. Wang, Y. Zhou, X. Zhang, B. Sun, G. Wang, et al., Photoelectrochemical biosensing platform for microRNA detection based on in situ producing electron donor from apoferritin-encapsulated ascorbic acid, Biosens. Bioelectron. 53 (2014) 175–181. doi:https://doi.org/10.1016/j.bios.2013.09.053.

[5] M. Wang, H. Yin, N. Shen, Z. Xu, B. Sun, S. Ai, Signal-on photoelectrochemical biosensor for microRNA detection based on Bi2S3 nanorods and enzymatic amplification, Biosens. Bioelectron. 53 (2014) 232–237. doi:https://doi.org/10.1016/j.bios.2013.09.069.

[6] H. Yin, Y. Zhou, B. Li, X. Li, Z. Yang, S. Ai, et al., Photoelectrochemical immunosensor for microRNA detection based on gold nanoparticles-functionalized g-C3N4 and anti-DNA:RNA antibody, Sensors Actuators B Chem. 222 (2016) 1119–1126. doi:https://doi.org/10.1016/j.snb.2015.08.019.

[7] B. Li, X. Li, M. Wang, Z. Yang, H. Yin, S. Ai, Photoelectrochemical biosensor for highly sensitive detection of microRNA based on duplex-specific nuclease-triggered signal amplification, J. Solid State Electrochem. 19 (2015) 1301–1309. doi:10.1007/s10008-015-2747-5.

[8] M. Wang, Z. Yang, Y. Guo, X. Wang, H. Yin, S. Ai, Visible-light induced photoelectrochemical biosensor for the detection of microRNA based on Bi2S3 nanorods and streptavidin on an ITO electrode, Microchim. Acta. 182 (2015) 241–248. doi:10.1007/s00604-014-1324-4.

[9] H. Cao, S. Liu, W. Tu, J. Bao, Z. Dai, A carbon nanotube/quantum dot based photoelectrochemical biosensing platform for the direct detection of microRNAs, Chem. Commun. 50 (2014) 13315–13318. doi:10.1039/C4CC06214K.

[10] J.M. Pingarrón, P. Yáñez-Sedeño, A. González-Cortés, Gold nanoparticle-based electrochemical biosensors, Electrochim. Acta. 53 (2008) 5848–5866.

doi:https://doi.org/10.1016/j.electacta.2008.03.005.

[11] A. Walcarius, S.D. Minteer, J. Wang, Y. Lin, A. Merkoci, Nanomaterials for bio-functionalized electrodes: recent trends, J. Mater. Chem. B. 1 (2013) 4878–4908. doi:10.1039/C3TB20881H.

[12] A.P. Xagas, M.C. Bernard, A. Hugot-Le Goff, N. Spyrellis, Z. Loizos, P. Falaras, Surface modification and photosensitisation of TiO2 nanocrystalline films with ascorbic acid, J. Photochem. Photobiol. A Chem. 132 (2000) 115–120. doi:https://doi.org/10.1016/S1010-6030(00)00202-1.

[13] G.-L. Wang, J.-J. Xu, H.-Y. Chen, Dopamine sensitized nanoporous TiO2 film on electrodes: Photoelectrochemical sensing of NADH under visible irradiation, Biosens. Bioelectron. 24 (2009) 2494–2498. doi:https://doi.org/10.1016/j.bios.2008.12.031.

[14] W. Tu, Y. Dong, J. Lei, H. Ju, Low-Potential Photoelectrochemical Biosensing Using Porphyrin-Functionalized TiO2 Nanoparticles, Anal. Chem. 82 (2010) 8711–8716. doi:10.1021/ac102070f.

[15] W. Lu, Y. Jin, G. Wang, D. Chen, J. Li, Enhanced photoelectrochemical method for linear DNA hybridization detection using Au-nanopaticle labeled DNA as probe onto titanium dioxide electrode, Biosens. Bioelectron. 23 (2008) 1534–1539. doi:https://doi.org/10.1016/j.bios.2008.01.011.

[16] W.-W. Zhao, Z.-Y. Ma, J.-J. Xu, H.-Y. Chen, In Situ Modification of a Semiconductor Surface by an Enzymatic Process: A General Strategy for Photoelectrochemical Bioanalysis, Anal. Chem. 85 (2013) 8503–8506. doi:10.1021/ac402523p.

[17] T. Rajh, J.M. Nedeljkovic, L.X. Chen, O. Poluektov, M.C. Thurnauer, Improving Optical and Charge Separation Properties of Nanocrystalline TiO2 by Surface Modification with Vitamin C, J. Phys. Chem. B. 103 (1999) 3515–3519. doi:10.1021/jp9901904.

[18] P.M. Sirimanne, T. Soga, Fabrication of a solid-state cell using vitamin C as sensitizer, Sol. Energy Mater. Sol. Cells. 80 (2003) 383–389. doi:https://doi.org/10.1016/j.solmat.2003.07.002.

[19] T. Placido, E. Fanizza, P. Cosma, M. Striccoli, M.L. Curri, R. Comparelli, et al., Electroactive Layer-by-Layer Plasmonic Architectures Based on Au Nanorods, Langmuir. 30 (2014) 2608–2618. doi:10.1021/la402873c.

[20] T. Placido, R. Comparelli, F. Giannici, P.D. Cozzoli, G. Capitani, M. Striccoli, et al., Photochemical Synthesis of Water-Soluble Gold Nanorods: The Role of Silver in Assisting Anisotropic Growth, Chem. Mater. 21 (2009) 4192–4202.

doi:10.1021/cm900721r.

[21] I. Palchetti, S. Laschi, G. Marrazza, M. Mascini, Electrochemical imaging of localized sandwich DNA hybridization using scanning electrochemical microscopy, Anal. Chem. 79 (2007). doi:10.1021/ac070474h.

[22] K. Gelderman, L. Lee, S.W. Donne, Flat-Band Potential of a Semiconductor: Using the Mott–Schottky Equation, J. Chem. Educ. 84 (2007) 685. doi:10.1021/ed084p685.

[23] J.D. Benck, B.A. Pinaud, Y. Gorlin, T.F. Jaramillo, Substrate Selection for Fundamental Studies of Electrocatalysts and Photoelectrodes: Inert Potential Windows in Acidic, Neutral, and Basic Electrolyte, PLoS One. 9 (2014) e107942. https://doi.org/10.1371/journal.pone.0107942.

[24] L. Kavan, M. Grätzel, S.E. Gilbert, C. Klemenz, H.J. Scheel, Electrochemical and Photoelectrochemical Investigation of Single-Crystal Anatase, J. Am. Chem. Soc. 118 (1996) 6716–6723. doi:10.1021/ja954172l.

[25] E.A. Johanna Löberg, Jenny Perez Holmberg, Ingela Mattisson, Anna Arvidsson, 139615, Int. J. Dent. 14 (2013). doi:10.1155/2013/139615.

[26] R. De Gryse, W.P. Gomes, F. Cardon, J. Vennik, On the Interpretation of Mott-Schottky Plots Determined at Semiconductor/Electrolyte Systems, J. Electrochem. Soc. . 122 (1975) 711–712. doi:10.1149/1.2134298.

[27] P.J. Mohr, B.N. Taylor, D.B. Newell, CODATA recommended values of the fundamental physical constants: 2006, Rev. Mod. Phys. 80 (2008) 633–730. https://link.aps.org/doi/10.1103/RevModPhys.80.633.

[28] B. Munirathinam, R. Narayanan, L. Neelakantan, Electrochemical and semiconducting properties of thin passive film formed on titanium in chloride medium at various pH conditions, Thin Solid Films. 598 (2016) 260–270. doi:https://doi.org/10.1016/j.tsf.2015.12.025.

[29] C. Baumanis, D.W. Bahnemann, TiO2 Thin Film Electrodes: Correlation between Photocatalytic Activity and Electrochemical Properties, J. Phys. Chem. C. 112 (2008) 19097–19101. doi:10.1021/jp807655a.

[30] J. Wu, H. Xu, W. Yan, Photoelectrocatalytic degradation Rhodamine B over highly ordered TiO2 nanotube arrays photoelectrode, Appl. Surf. Sci. 386 (2016) 1–13. doi:https://doi.org/10.1016/j.apsusc.2016.05.155.

[31] B.P. Khanal, E.R. Zubarev, Rings of Nanorods, Angew. Chemie Int. Ed. 46 (2007) 2195–2198. doi:10.1002/anie.200604889.

[32] N. Haddour, J. Chauvin, C. Gondran, S. Cosnier, Photoelectrochemical Immunosensor for Label-Free Detection and Quantification of Anti-cholera Toxin Antibody, J. Am. Chem. Soc. 128 (2006) 9693–9698. doi:10.1021/ja062729z.

[33] W.-W. Zhao, Z.-Y. Ma, D.-Y. Yan, J.-J. Xu, H.-Y. Chen, In Situ Enzymatic Ascorbic Acid Production as Electron Donor for CdS Quantum Dots Equipped TiO2 Nanotubes: A General and Efficient Approach for New Photoelectrochemical Immunoassay, Anal. Chem. 84 (2012) 10518–10521. doi:10.1021/ac3028799.

[34] F. Bettazzi, E. Hamid-Asl, C. Esposito, C. Quintavalle, N. Formisano, S. Laschi, et al., Electrochemical detection of miRNA-222 by use of a magnetic bead-based bioassay, Anal. Bioanal. Chem. 405 (2013) 1025–1034. doi:10.1007/s00216-012-6476-7.

[35] D. Voccia, F. Bettazzi, E. Fratini, D. Berti, I. Palchetti, Improving impedimetric nucleic acid detection by using enzyme-decorated liposomes and nanostructured screen-printed electrodes, Anal. Bioanal. Chem. 408 (2016) 7271–7281. doi:10.1007/s00216-016-9593-x.

[36] D. Voccia, F. Bettazzi, G. Baydemir, I. Palchetti, Alkaline-Phosphatase-Based Nanostructure Assemblies for Electrochemical Detection of microRNAs, J. Nanosci. Nanotechnol. 15 (2015) 3378–3384. doi:doi:10.1166/jnn.2015.10201.

Figures

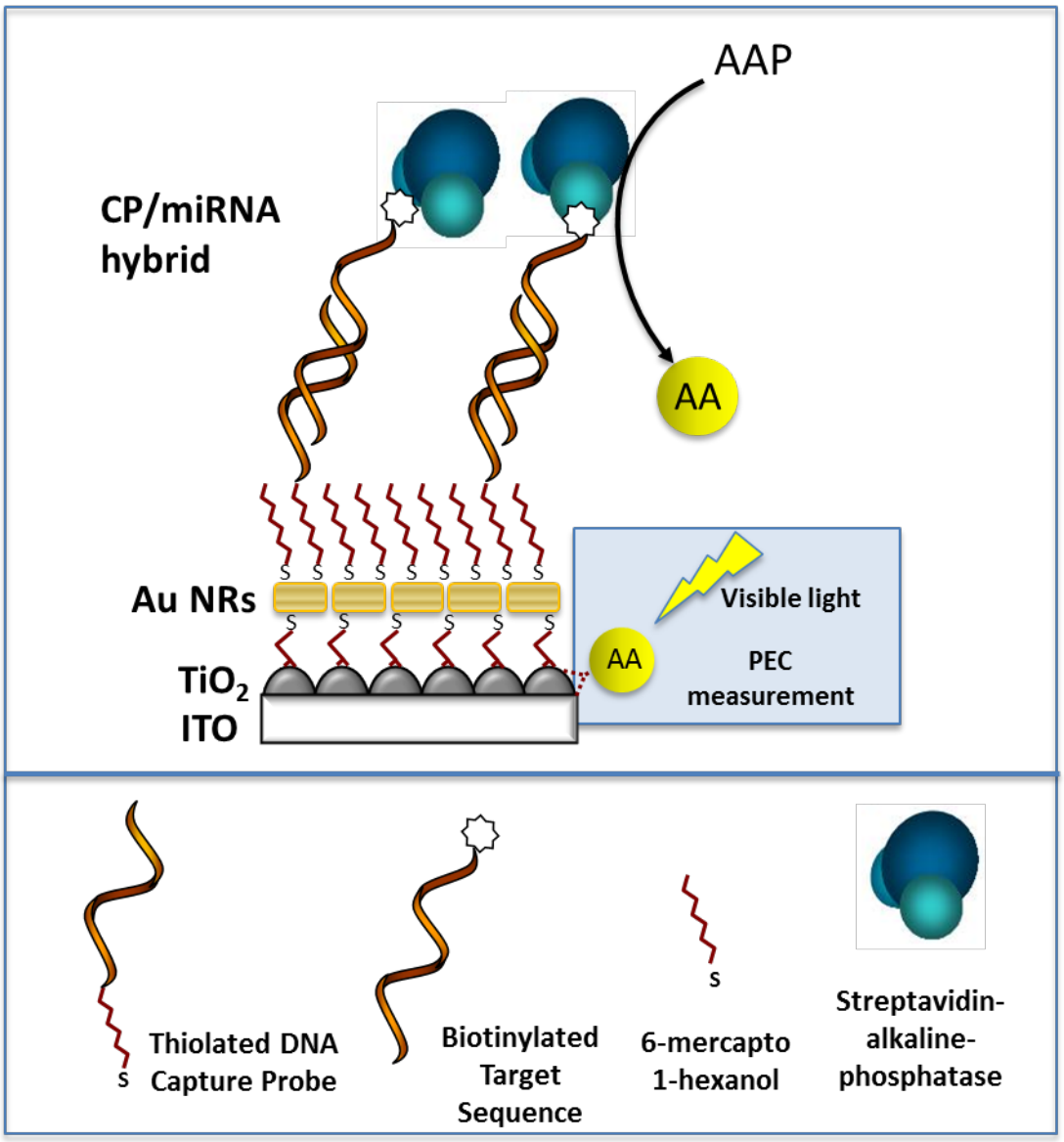

Scheme 1: Scheme of the assay: AuNRs/MSA/TiO_2/ITO electrodes are, first, exposed to a solution containing the thiolated oligonucleotide, followed by an incubation with mercaptohexanol. The probe-modified electrode is then exposed to a solution of the biotinylated target sequence. The biotinylated hybrid obtained at the electrode surface is reacted with a solution containing the streptavidin-alkaline phosphatase conjugate. The enzyme catalytic activity converts L-ascorbic acid 2-phosphate (AAP) in ascorbic acid (AA). AA, through the formation of a charge-transfer complex, shift the onset of photocurrents in

the visible spectral region.

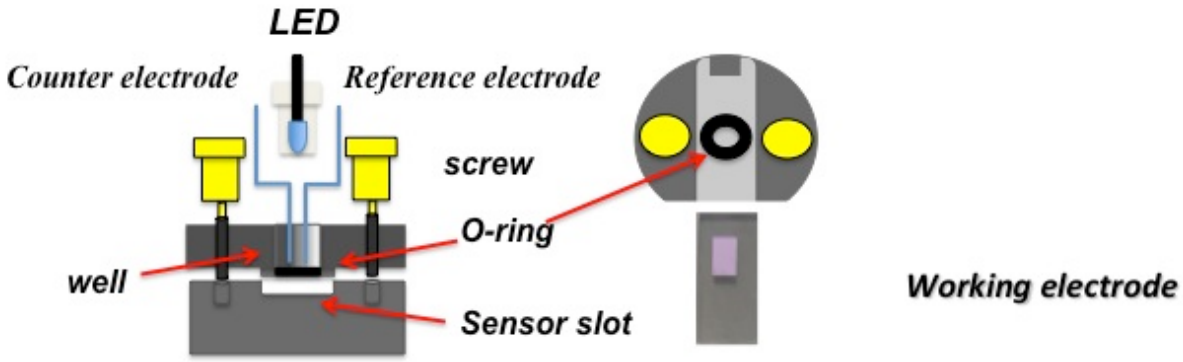

Scheme 2: Scheme of the photoelectrochemical cell

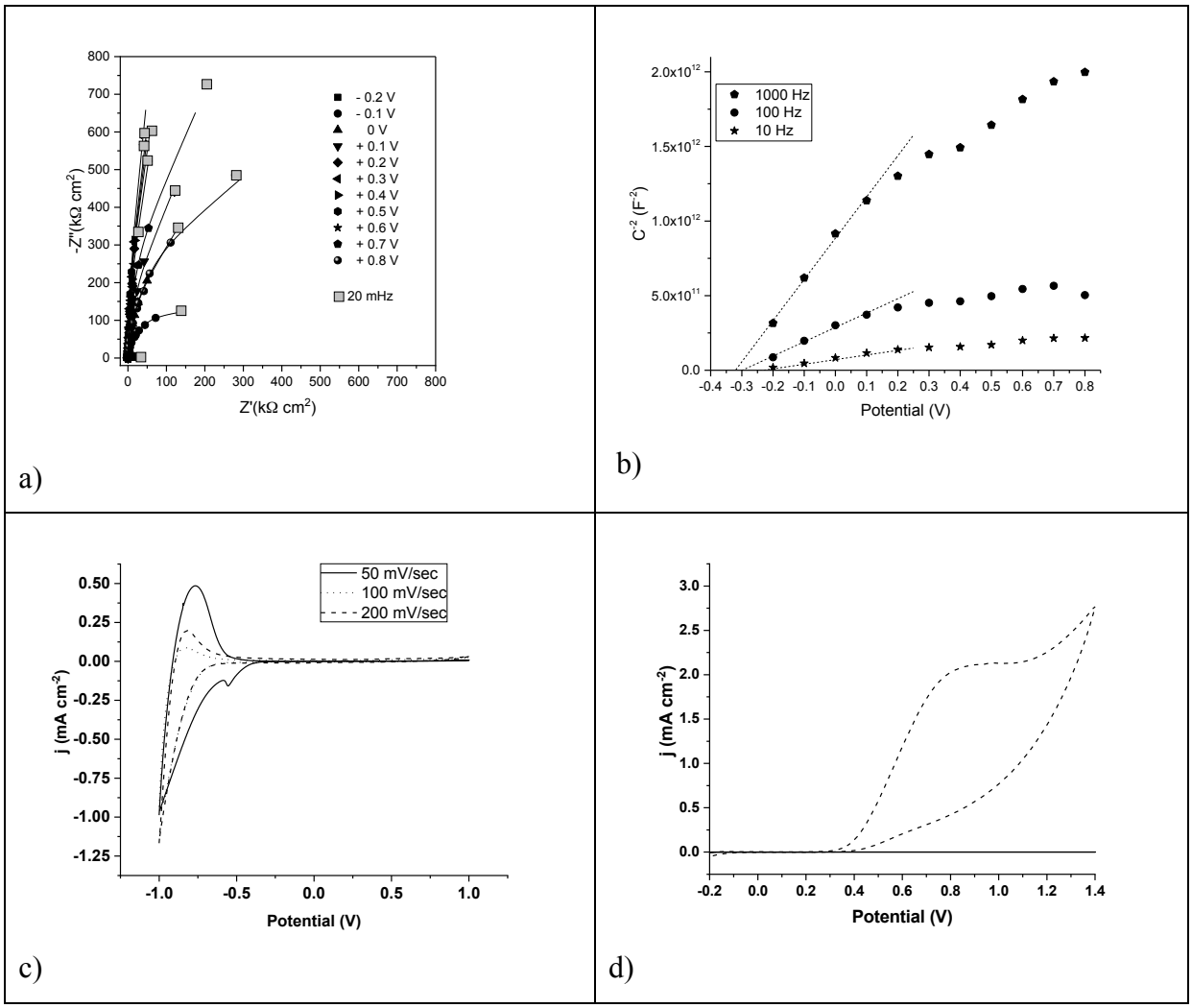

Figure 1: Electrochemical Characterization of the TiO_2/ITO electrode: a) Nyquist plots recorded in 0.1 M KCl at TiO_2/ITO electrode from -0.2 to +0.8 V *vs.* Ag/AgCl; experimental data are expressed as points, while lines represent the obtained equivalent circuit fitting; b) Mott–Schottky plot for TiO_2/ITO electrode in 0.1 M KCl solution, at 1000, 100, 10 Hz, respectively; c) CVs recorded from - 1.0 to +1.0 V vs. Ag/AgCl, at different scan rate, in 0.1 M KCl at TiO_2/ITO electrode; d) CVs recorded from -0.2 to +1.4 V vs. Ag/AgCl, at 50 mV/s, in 0.1 M KCl in presence (dashed line) and absence (solid line) of 10 mM AA.

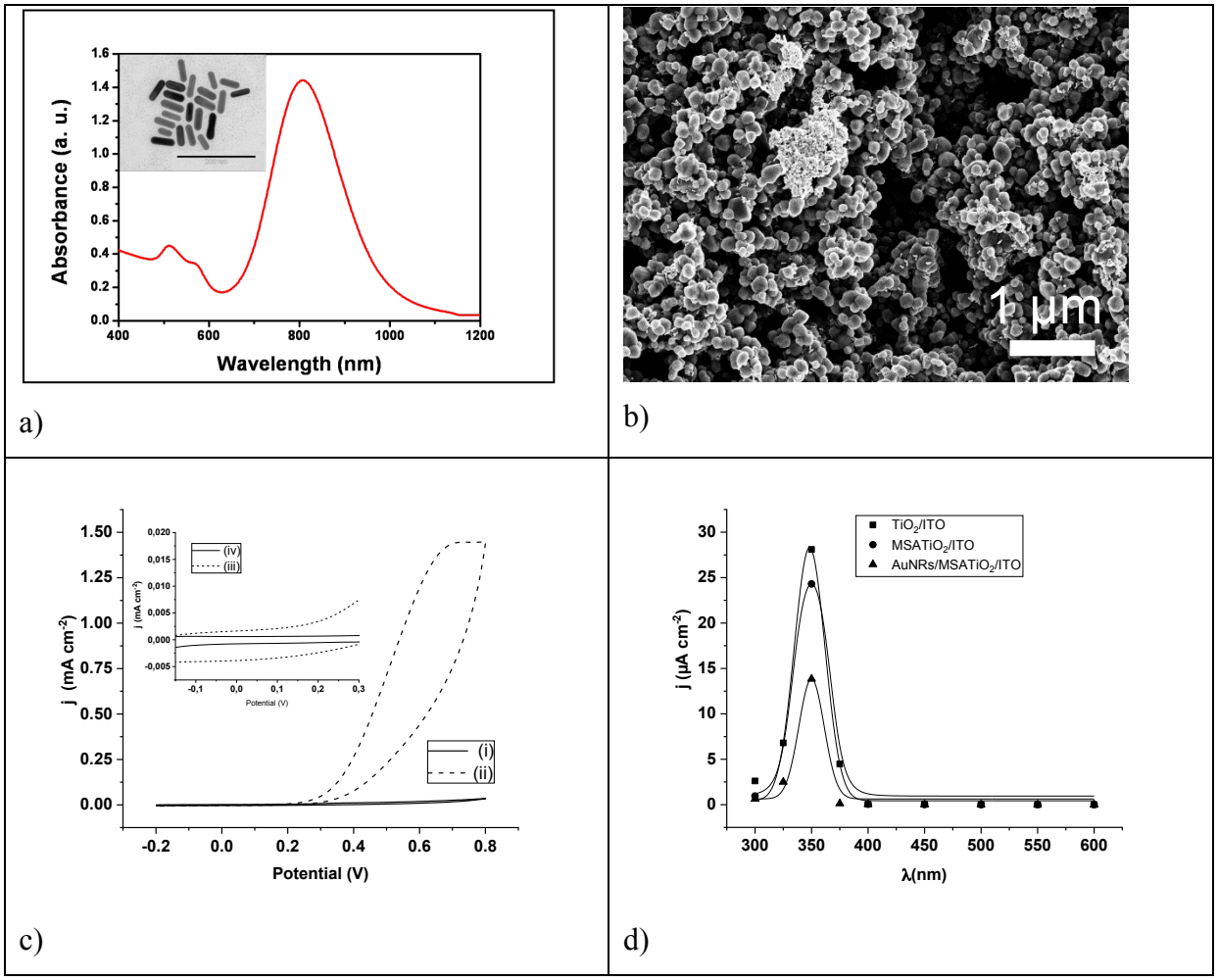

Figure 2: UV-vis-NIR absorption spectroscopy, SEM and electrochemical characterization of the AuNRs/MSA/TiO_2/ITO electrode: a) AuNRs absorption spectrum, recorded from 400 to 1200 nm in toluene. The inset shows the TEM micrograph of synthesized Au NRs; b) SEM micrograph of the AuNRs/MSA/TiO_2/ITO electrode (acceleration voltage of 3.0 kV and magnification of 46530 X and with an aperture size of 30 µm); c) CVs recorded at AuNRs/MSA/TiO_2/ITO electrode in 0.1 M KCl, scan rate 50 mV/s in absence (i) and presence (ii) of 10 mM AA, in dark (the inset show an enlargement of the CVs recorded at AuNRs/MSA/TiO_2/ITO (iii) and MSA/TiO_2/ITO electrode (iv), respectively, in the range -0.1 to + 0.3 V, scan rate 50 mV/s); d) Photocurrents recorded at AuNRs/MSA/TiO_2/ITO, MSA/TiO_2/ITO, TiO_2/ITO electrodes in 10 mM Tris buffer, pH 9.8 at 0 V vs Ag/AgCl, under illumination from 300 to 600 nm.

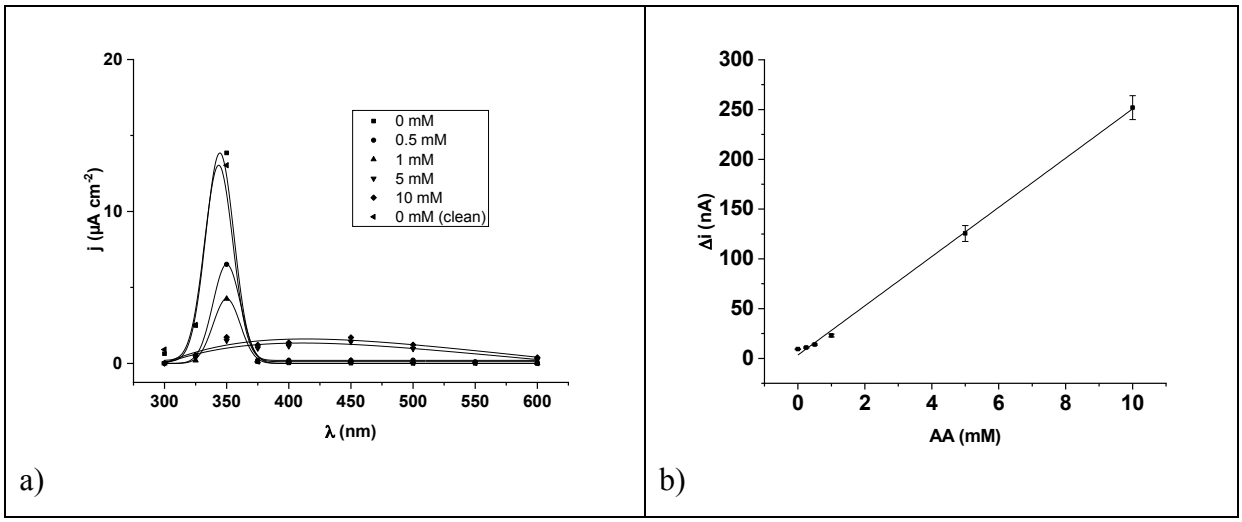

Figure 3: Evaluation of AA concentration on photocurrent values: a) Photocurrent response in presence of different concentration of AA corresponding to 0, 0.5, 1, 5, 10 mM, respectively. Photocurrent recorded in 0 mM AA after a washing step with demineralized water (-◄-) was also reported. Excitation light from 300 to 600 nm. The AuNRs/MSA/TiO_2/ITO electrode was exposed to increased concentration of AA in 10 mM Tris buffer (pH=9.8); b) PEC calibration plot of AA, recorded in 10 mM Tris buffer (pH=9.8), at a constant potential of 0 V and using a commercial white LED light.

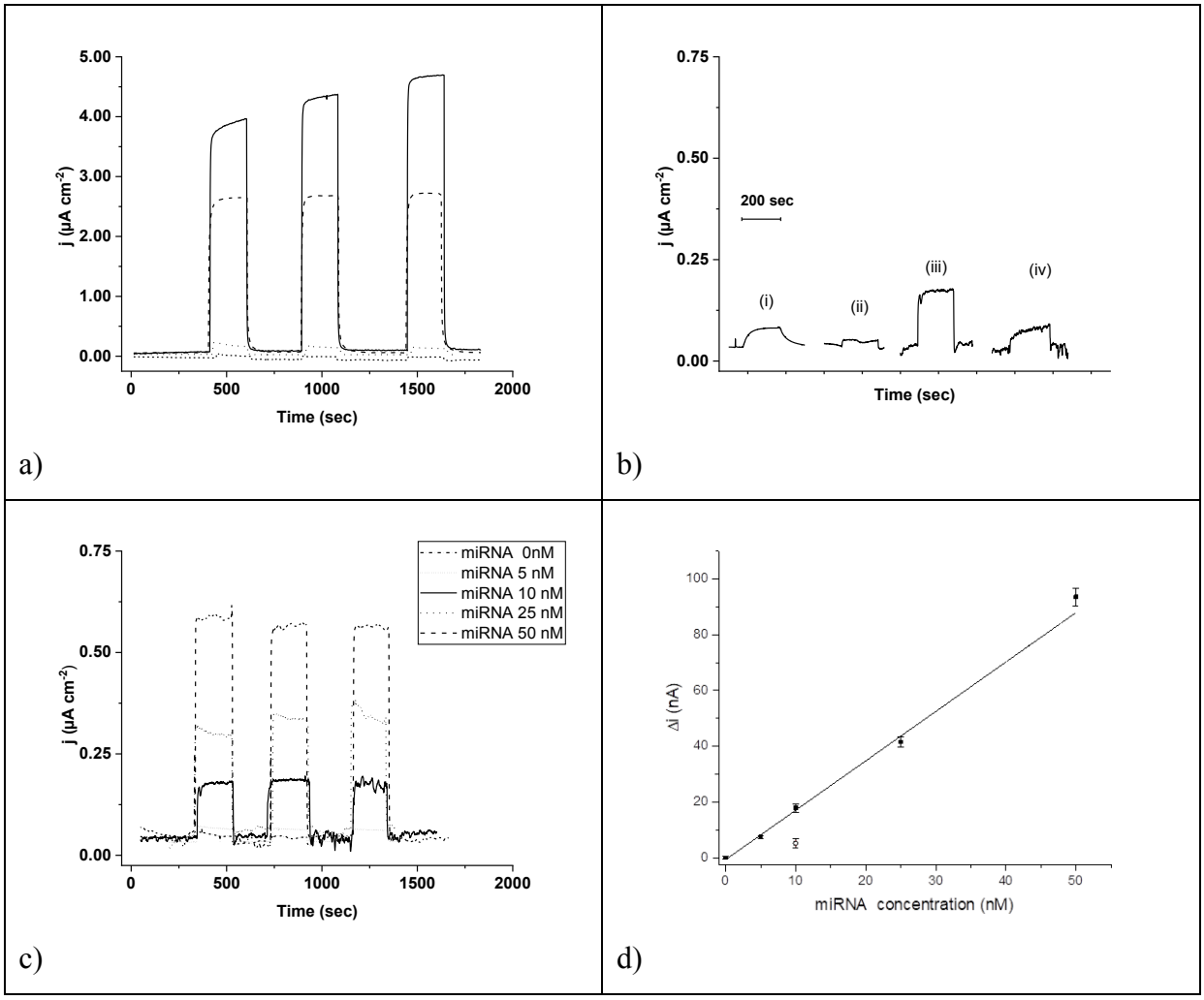

Figure 4: Photoelectrochemical characterization of the genosensor: a) Photocurrents recorded at the bare AuNRs/MSA/TiO_2/ITO electrode in presence (solid line) and absence (dotted line) of 10 mM AA in 10 mM Tris pH=9.8, and photocurrents recorded at CP-modified-AuNRs/MSA/TiO_2/ITO electrode in presence (dashed line) and absence (short dashed line) of 10 mM AA in 10 mM Tris pH=9.8; b) photocurrents recorded at the bare AuNRs/MSA/TiO_2/ITO electrode (i) in 10 mM Tris (pH=9.8) and at ALP–10 nM miRNA-CP-modified-AuNRs/MSA/TiO_2/ITO electrode in presence (iii) and absence (ii) of 10 mg/mL AAP in 10 mM Tris pH=9.8, and at the same electrode after washing and in presence of 10 mg/mL AAP in 0.5 M PB (iv); c) photocurrents recorded in presence of increased concentration of microRNA target (0, 5, 10, 25, 50 nM). Data are recorded at 0 V vs Ag/AgCl in 10 mM Tris (pH=9.8) in presence of 10 mg/mL AAP. Further details are reported in the material and methods section. d) Corresponding calibration plot, were the photocurrent value of a non complementary microRNA sequence was also reported (O). Each point

represents the mean of at least three measurements and the error bars the corresponding standard deviation.